International Journal of Hydrogen Energy 65 (2024) 83–94

Contents lists available at ScienceDirect

International Journal of Hydrogen Energy

journal homepage: www.elsevier.com/locate/he

System dynamics of polymer electrolyte membrane water electrolyzers and impact of renewable energy sources on systems design

Edward Rauls [a], Michael Hehemann [a], Fabian Scheepers [a], Martin Müller [a,**], Ralf Peters [a,d], Detlef Stolten [b,c]

[a] Forschungszentrum Juelich GmbH, Institute of Energy and Climate Research, IEK-14: Electrochemical Process Engineering, 52425, Juelich, Germany
[b] Forschungszentrum Juelich GmbH, Institute of Energy and Climate Research, IEK-3: Techno-economic System Analysis, 52425, Juelich, Germany
[c] RWTH Aachen University, Chair for Fuel Cells, Germany
[d] Synthetic Fuels, Institute for Fluid- and Thermodynamics, Ruhr-Universität Bochum, Universitätsstr. 150, Bochum 44801, Germany

ARTICLE INFO

Handling Editor: Søren Juhl Andreasen

Keywords:
PEM electrolysis
Dynamic operation
Green hydrogen
Experimental investigation

ABSTRACT

Water electrolyzers will ensure energy security and power grid stability in energy systems based on fluctuating renewable energy sources such as wind power and photovoltaics. In this article, the effects of volatile energy generation on the operating conditions within polymer electrolyte membrane water electrolyzers are investigated. Based on experiments on a 100 kW_{el} test station, it is concluded that isothermal and isobaric operation is unattainable and temperature deviations between −7 K and 3 K from their setpoint are observed. Pressure control on the hydrogen side is more challenging than on the oxygen side. Temperature decreases due to non-ideal temperature control overall decrease the mean efficiency during dynamic operation as compared to steady-state, with wind power reaching 73.70 $\%_{LHV}$ and solar power yielding 71.90 $\%_{LHV}$. Finally, adaptions of electrolyzer designs and operation strategies are discussed, that could reduce negative effects of system dynamics on process efficiency.

1. Introduction

Future energy systems may be mainly based on renewable energy sources (RES) such as wind power and photovoltaics (PV) to reduce the dependency on anthropogenic climate change inducing carbon containing energy carriers such as coal and oil [1]. Contrary to the currently predominately used fossil fuels, RES exhibit two main operational characteristics: intermittency and variability. Intermittency describes the discontinuous and temporally limited availability of energy due to their dependency on the weather, which poses challenges to grid stability [2]. At times, renewable energy (RE) may only be available to an extent that is insufficient to meet energy demands across all energy applications. To ensure reliable energy supply during these periods, production capacities of RES must be oversized to produce sufficient storable surplus energy during times of energy availability [3]. Variability describes the inherent dynamic supply of energy from non-dispatchable RES [4]. Although the quality of weather predictions has improved substantially in recent years, short-term regional fluctuations of RES – for example due to cloud movement or local turbulences – have a direct influence on local grid stability [5]. Electricity grid interconnection and distribution of generation sites have smoothing effects, but the dynamics of nature can never be fully diminished [6].

For the power system to be stable, the residual load, that is the difference between electricity demand and supply, must be contained within acceptable limits, which currently primarily is covered by controllable thermal power plants [7]. Progressing electrification and sector coupling will aggravate the stresses on stakeholders of the electricity sector as electricity will become the prime energy vector in near carbon-neutral energy systems [8]. Detrimental fluctuations of grid frequency and voltage in systems with high shares of variable RE can be avoided by ensuring sufficient grid flexibility through demand side management strategies and energy storage [9]. Energy storage systems must meet certain criteria to be able to contribute to grid stability. Milligan [10] lists three principal prerequisites as: physical ability, operating state that allows activation, and economic incentive to provide grid services. In a recent study, relevant grid codes for the provision of grid services by PEM electrolyzers were analyzed [11]. In other experimental studies, the behavior of electrolyzers under dynamic load

** Institute of Energy and Climate Research, Electrochemical Process Engineering (IEK-14), Forschungszentrum Jülich GmbH, 52425, Jülich, Germany
E-mail address: mar.mueller@fz-juelich.de (M. Müller).

https://doi.org/10.1016/j.ijhydene.2024.03.302
Received 17 November 2023; Received in revised form 8 March 2024; Accepted 24 March 2024
Available online 4 April 2024

profiles were investigated. Bergen et al. [12] report significant efficiency losses in dynamic operation of an alkaline electrolyzer at lab scale. Sartory et al. examined step responses of up to 100 kW_{el} from different operating states and concluded from the experiments, that the flexibility of the electrolyzer was sufficient for intermittent operation [13]. If directly coupled to PV modules, solar-to-hydrogen efficiencies above 10 % were reported [14].

Direct coupling of water electrolyzers to RES has been demonstrated in many projects throughout the world. Early projects were focused on island systems and used alkaline electrolyzers directly coupled to PV panels [15] or wind turbines [16]. Limitations to the load following capacities of alkaline electrolyzers were observed [17]. Therefore, many recent demonstrators use Polymer Electrolyte Membrane (PEM) water electrolyzers that are operated under characteristic loads from wind power or PV [18]. The ability of PEM electrolyzers follow intermittent energy inputs was proven relatively early, but stack and cell degradation issues were also reported, however without identifying the actual degradation mechanisms [19]. Including an intermediate battery storage can lengthen the operation times and increase the duty factor of electrolyzers in island systems further [20]. Lately, at Energiepark Mainz, Germany, a 6 MW_{el} PEM electrolyzer demonstrated the ability to perform ancillary grid services at grid scale in close proximity to wind power systems [21].

In this article a quantitative analysis of transient operating states and their implications on the overall efficiency for coupling to RES are examined. To the best of the authors knowledge, it is the first article to examine the effect of water expulsion from the electrolysis stacks after substantial load changes based on mathematical equations. This effect has multiple effects on the performance at the stack and system level, such as pressure control and efficiency due to internal gas crossover. Furthermore, this article allows a direct comparison of the effects of different coupling scenarios, whereas other publications focus more on one specific RES and do not offer quantitative comparisons of the rates of change for all operating conditions. Finally, potential strategies for adaptions of electrolyzer design and operation are discussed, which may help to reduce negative effects of system dynamics. To highlight the impact of each system component on the flexibility of the electrolyzer, a technical analysis ranging from the cell to the system levels is presented.

1.1. Electrolysis system configuration

PEM water electrolyzers consist of multiple typical components that act interconnectedly to produce hydrogen electrochemically from water and electricity. In the following section a system analysis is conducted to identify the influence of these components on the dynamic operability of the entire electrolyzer. Electrical power is supplied by the power supply at the desired levels. In case of an AC grid connection, a combination of an alternate current (AC) transformer and an AC/DC rectifier is necessary [22]. The cell stack is the central component of PEM electrolyzers and determines their power rating, efficiency, and the overall system design. Perfluorosulfonic acid (PFSA) membranes such as Nafion™ are used in PEM electrolyzers. They separate anode and cathode by electrically insulating the electrodes, while conducting ions and separating the product gases. At the anode side, water is turned into oxygen gas and protons, additionally releasing two electrons per water molecule. Concurrently, protons are conducted over the membrane and reduced to molecular hydrogen. During the migration of the protons through the membrane, water is drawn from anode to cathode side due to electrostatic attraction [23]. These water losses from this so-called electroosmotic drag must be replenished at the anode by a feed pump, while excess water must be removed at the cathode.

Water acts simultaneously as a reactant and as the thermal medium. It leaves the stack enriched with product gases that are removed gravimetrically in gas-water separators. Recirculation pumps subsequently push the water through a heat exchanger, an ion exchanger, and a heating element before the water reenters the stack. The ion exchangers in the water cycle remove foreign ions from the process water to prevent accelerated membrane degradation. Foreign ions may originate from metal piping or stack components and cause accelerated cell degradation through membrane poisoning [24]. Heat exchangers and heating elements are used to control the operating temperature within the stack. The reference electrolysis system of this manuscript encompasses separate water cycles for the anodic and the cathodic compartments, see Fig. 1 a). However, many electrolyzers operate with anodic water supply only [25], as shown in Fig. 1 b). Operation with solely cathodically supplied cells is also possible, which is especially suited to electrolyzers with thin membranes and exhibits limited power densities than anodically supplied systems [26].

2. System analysis: technical limitations to dynamic operation

Electrolysis cell stacks are complex systems, in which transport processes of electrical charge, chemical species, and heat occur simultaneously during hydrogen production. Implicitly, limiting factors to dynamic operation amongst others are electrical load-following, media and thermal management, and cell degradation.

2.1. Dynamic behavior of the cell stack

The electrical load following capabilities of PEM electrolyzers have mostly been investigated on single cells. Immerz et al. [27] report the ability for setpoint changes in less than 1 ms and stabilization of the power at the new steady conditions within 3 s for galvanostatic and potentiostatic operation respectively. Mohanpurkar et al. [28] report sub-second response and settling times of a 120 kW_{el} electrolysis stack based on experiments. These time constants partly depend on the electrochemical properties of the stack components but also on the control of the power supply employed for the experiments.

Satisfactory mass transport of water to the reactive sites at the anode catalyst and removal of reaction gas streams from both catalyst layers must be ensured to avoid mass transport resistances [25]. Therefore, internal stack components such as bipolar plates and porous transport layers (PTLs) must be well designed. Bipolar plates mechanically support the membrane electrode assembly and provide electrical contact between the cells in conjunction with the PTLs. Additionally, they facilitate the water supply of the reactive sites and the removal of the produced gases therefrom [29]. Based on in situ neutron radiography experiments, Panchenko et al. recommend stoichiometries between 350 and 600 in relation to the molar water requirement of the electrochemical reaction, to guarantee efficient gas removal and avoid congestion of reactive sites [30]. In addition to gas removal, the water stoichiometry should sustain adequate heat removal from the reactive sites to prevent thermal degradation of the PFSA membrane due to hot spot formation [31].

Dynamic and intermittent electrolyzer operation has been reported to cause accelerated cell degradation [32]. While the underlying mechanisms are not yet fully understood, several promising explanations and even mitigation strategies have been proposed in recent years. General causes for performance losses of PEM electrolysis cells are membrane thinning and pinhole formation, cation contamination of the membrane, and passivation of the Titanium PTL [33]. Alia et al. [34] observe increased performance losses because of cycling stresses. They suggest that Iridium dissolution and subsequent anode catalyst layer thinning due to load switching cause this performance decrease. However, they also find that wind and PV load profiles lead to lower degradation, as they are less aggressive than synthetic saw tooth or rectangular profiles [34]. Frensch et al. observe increased fluoride emission during intermittent operation, pointing at degradation of the Nafion™ membrane and catalyst binder material [35]. Rakousky et al. observe cell degradation at 1.84 V but not at 1.70 V and recommend avoiding frequent current interruptions [32]. Weiβ et al. identify the anode catalyst layer as the principal degradation center. Switching

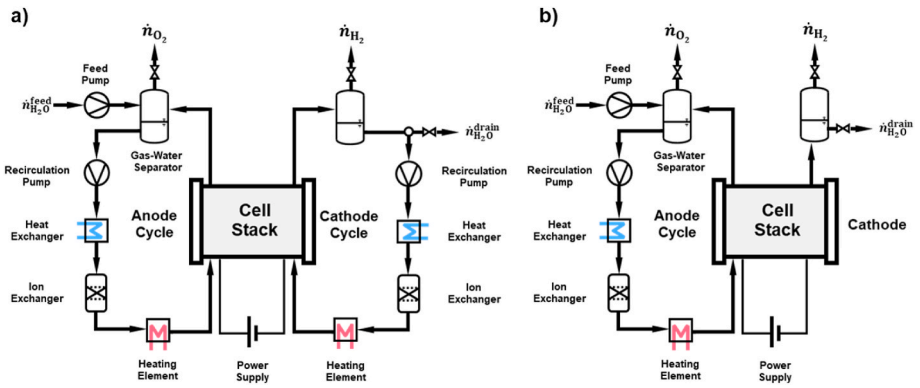

Fig. 1. Process structures of polymer electrolyte membrane water electrolyzers: a) with water circulation on the anode and cathode side; b) with water circulation only on the anode side.

between oxidizing conditions during operation and reducing conditions during current interruptions leads to increased Iridium dissolution and performance losses in terms of catalyst activity. With the general trend towards thinner membranes and reduced catalyst loadings, especially at the anode, further research focused on understanding and reducing cell degradation during intermittent operation are necessary. Operation of electrolyzers at a minimal load is suggested to avoid the negative impact of current interruptions [33]. However, in that case a recombination catalyst is needed to remove permeated hydrogen from the oxygen stream, causing higher investment costs.

2.2. Dynamic behavior of the peripherals

Although the responsiveness of PEM water electrolysis stacks to electrical load shifts is high, the entire system may be substantially slower due to the inertia of auxiliary components. Table 1 gives an overview of typical response times for different components of water electrolyzers.

Electrical load following capabilities depend on the technologies of process control and power supply. Both quantities allow setpoint changes in the sub-second because of the high transfer speed of digital signals and electrical charges in solid state materials, respectively. The load following ability of the power supply depends on the utilized power supply architecture and control [36]. Thyristor-based rectifiers are currently the main choice for water electrolyzers because of the required high currents, although their disadvantages such as the generation of reactive power and substantial current ripples [37]. High current ripple content of electrolyzer power input increases the specific energy demand [38] and necessitates active and passive filters, adding to complexity, cost and volume of the power supply [37].

Table 1
Time constants and functions of electrolyzer components, based on operational experience.

	Function	Component	Dimension
Information	Signal transmission	Process control devices	ms
Electrical	Power conditioning	Power supply	ms
	Cell polarization	Stack	< s
Thermal	Temperature control	Stack	s - min
		System	min - h
Fluids – liquid	Flow control	Pumps, Piping, Filters, Stack	s
	Volume control	Separators, Vessels	s - min
Fluids – gaseous	Pressure control	Separators, Vessels, Valves	s - min
	Gas conditioning	Dryer, Compressor	s - min

2.2.1. Water management and process control

Gas-water separators buffer the system behavior and dampen the system dynamics to an extent. Besides the removal of liquid from the electrolysis product streams, they also influence the operating pressure, pressure build-up, and the thermal behavior of the electrolyzer. Separator vessels are only partially filled with liquid to accommodate for potential changes in water flow rates. In case of rapid upwards changes of water flow rates, low filling volumes may lead to gas drag to the pumps, causing damage to equipment and disturbance of the process. Fig. 2 depicts the source of water surges in PEM electrolysis systems and its implications on the operating conditions. During electrolysis, the cell stack contains a gaseous and a water fraction whose composition is operating point dependent at fixed water flow rates. At increasing electrical power densities, more water is split into hydrogen and oxygen from a fixed water flow rate, thereby expanding the gas content of the stack and expelling a corresponding water volume. Upward load changes, defined as switching from a lower power density (Fig. 2, State 1) to a higher power density (Fig. 2, State 2), incurs upward water surges in the separator vessels because of this water displacement by gas in the stack. Downward load point changes inversely induce falling separators as less water leaves the stack than before while the recirculation pump draws a fixed flow from the vessel. To maintain the water level within the separator vessels, operating point dependent level control is required. Fast changes of the water volume in the separators influence the gas pressure because the gas volume changes simultaneously. The gas release valve control consequently must consider these dynamic load changes to mitigate excessive pressure deviations.

Appropriate piping design is vital in the context of water management, as over dimensioning of pipes and separator vessels adds to the fluidic and thermal inertias of the electrolyzer and impedes temperature and pressure control. Feed-forward control can be used to compensate potential effects of sudden setpoint changes to stabilize stack temperatures and gas pressures [39]. Using such advanced control schemes, temperatures and pressures can be controlled within seconds or in case of severe setpoint changes minutes. Recirculation pumps that are operated by frequency drives can handle setpoint changes within seconds, but depending on their position relative to the stack, they may not be able to match sudden electric load changes. Fixed flow rate operation is therefore usually preferred over variable flow rate operation. Regarding the dynamic behavior of electrolyzers, the overall thermal system response is the slowest process. Heat is introduced by the cell stack and by a possible additional heating. While the electrolyzer heats up, the heat losses to the ambient increase, dampening the temperature response of the system further, leading to heat-up durations of up to several hours to reach the operating temperature after start-up [40].

2.2.2. Gas conditioning and storage

Further time shifts between production and delivery of hydrogen can

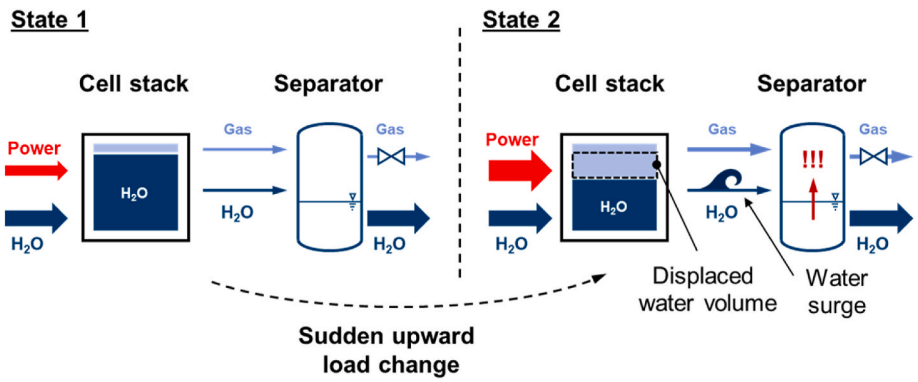

Fig. 2. Schematic explanation of the underlying mechanisms of water surges in polymer electrolyte water electrolyzers following substantial electrical load changes.

be caused by gas conditioning steps such as gas drying and compression. These time shifts have no influence on the ability of the electrolyzer to be operated dynamically, but rather on the availability of storable hydrogen at the product specifications. Drying of the hydrogen gas to specific humidity levels – via pressure swing adsorption [41] or temperature swing adsorption [42] – is independent from the gas input but adsorption of water vapor in silica bed entails certain gas retention times. Gas compressors, that contain moving parts such as reciprocating pistons or rotating screws, cannot be operated below certain specific gas flows [43]. Appropriate design of buffer gas storage vessels before the compressor prolongs operation periods and thereby reduces potential wear out of mechanical components. Additional storage capacity can serve as buffer between hydrogen production and subsequent utilization. The size of this storage depends on the electrolyzer application and coupling scenario. For example, the buffering of day-night-cycles in PtG plants that are directly coupled to PV installations requires larger storage capacities than in the case of coupling to wind power or grid stability service provision [44].

3. Materials and methods

3.1. Materials

System dynamics were examined on an electrolyzers test bench with a maximum electrical power rating of 100 kW_{el}. Two cell stacks with 27 cells each and a cell area of 300 cm^2 were operated in the test bench. Nafion™-117 membranes with a thickness of 183 µm were utilized as membrane material. The anode catalyst was iridium (2.6 mg cm^{-2}), and the cathode catalyst was platinum (0.9 mg cm^{-2}). Water circulation in the anode and cathode cycle was ensured by gear pumps at a constant flow rate of 15.75 l min^{-1}. The gas-water separator vessels had a volume of 9000 cm^3, with a filling level setpoint of 66 %. All experiments were performed at a temperature setpoint of 75 °C, gas pressures of 6 bar on the cathode, and 5 bar on the anode side. These gas pressure levels are required on the test station because of the utilized hydrogen in oxygen gas sensor, which requires these minimum pressures. The volume flow rate of hydrogen at normal conditions (0 °C; 1,01325 bar) is measured by a Bronkhorst® F-112 A C flow meter. Temperature control was realized by 36 kW_{th} plate heat exchangers (AlphaLaval) and 4 kW_{th} cartridge heaters (Türk + Hillinger). An insulated-gate bipolar transistor DC power supply (aixcon PowerSystems) provided the electrical power to the stacks, that were operated in galvanostatic mode.

3.2. Dynamic electrolyzer operation

To investigate the electrolyzer system dynamics in the context of renewable energy sources and grid stability services, characteristic load profiles were generated and run on the test bench. Table 2 gives an overview of the current density ranges, total profile duration and time resolution of the characteristic profiles. The time resolution of the data logging was limited to 2 s due to the installed hardware and the time resolution of the load profiles differed according to the available datasets. Regarding the relative installed power of the individual RES, it is assumed that power rating of the electrolyzer and the RES fully match.

Table 2
Properties of the characteristic load profiles used for the experiments. The absolute current density step height is calculated from the minimum and maximum difference between operating points of the load profile at the respective time resolution of the load profile.

		Step profile	Wind power	Photovoltaics
Current density step height	Δj (min./max.)	−1.90/1.90 A cm^{-2}	−0.15/0.37 A cm^{-2}	−0.93/0.88 A cm^{-2}
Duration	t (total)	6.5 h	5 h	14 h
Resolution	Δt (load profile)	10 min	1 s	1 min
	Δt (data logging)	2 s	2 s	2 s

3.2.1. Operating profiles from renewable energy sources

The first experiment simulated the scenario of water electrolyzers in baseload operation during the provision of grid stability services. Prequalification experiments have been presented at lab-scale in Ref. [11] or at MW scale in Ref. [21] for PEM electrolyzers. In this work, the response of PEM water electrolyzers to sudden load changes was investigated by subjecting it to a rectangular current density profile with increasing step heights. After a fixed interval of 10 min at a base current density 0.2 Acm^{-2}, an upward step was performed. The step height increment was 0.1 Acm^{-2}. Then, after 10 min at the increased current density, a downward step to the base current density followed and the procedure was repeated until a final step height of 1 Acm^{-2}.

Further experiments on the direct coupling of electrolyzers to RES were performed by exemplary load profiles from real life wind power and PV data. A wind profile with a total duration of 5 h in 1 Hz resolution was taken from Ref. [6]. Although this data set represents the total mechanical power, which corresponds directly to the wind speeds, and not the electrical output from the wind turbine, it can be applied to experiments at the 100 kW_{el} scale. The power output from small-scale wind turbines is more directly connected to wind speed variations than from large-scale wind turbines, since the interconnected inertia is smaller [45]. The length of the wind power profile is considered sufficient because it contains characteristic intervals of high and low absolute electric power, which correspond to respective windspeed conditions.

As the procurement of PV with high temporal resolution proved difficult, a day profile in 1 min resolution from the PHOEBUS

demonstrator project was used [15]. Higher time resolution should in principle lead to smoother load profiles for the electrolyzers because transient states are averaged during data logging at low time resolution. The applied PV profile therefore is not fully representative of direct coupling of PV panels and water electrolyzers. Nonetheless, this more aggressive load profile can be used to investigate the system reaction to harsh load changes. A full day is investigated to include effects of day-night-shifts.

3.2.2. Evaluation of the system response

The electrolyzer efficiency η_{el} is quantified in terms of the hydrogen production at a specific electrical power uptake P_{el}, as stated in (1). In this study, the efficiency is based on the volumetric lower heating value (LHV) of hydrogen ($LHV_{H_2} = 3$ kWh m^{-3} at normal conditions) and the measured normal gas flow rate $\dot{V}^{cat}_{H_2,norm}$ at the cathode side. For the evaluation of the experimental process efficiency, the gas flow data is averaged over 60 s to filter sensor noise and artificial gas flow discontinuities for example through load changes or water level control in the separators.

$$\eta_{el} = \frac{\dot{V}^{cat}_{H_2,norm} \cdot LHV_{H_2}}{P_{el}} \tag{1}$$

Following (2), the electrical power uptake of the electrolyzers results from the product of the stack voltage U_{stack} and the current I_{stack}, that is applied to the electrolysis cells. In electrolysis stacks, the cells are connected in series, which causes the stack voltage to scale with the number of cells n_{cell} based on the voltage U_{cell} of the individual cells, as stated in (**3**). Identical performance of all cells within the stacks is assumed in (**3**). For the evaluation of the experiments, the mean voltage was calculated from the single-cell voltage measurement data. Likewise, the current is equal in all cells and correlates with the current density j_{cell} by the geometric cell area as per (**4**).

$$P_{el} = U_{stack} \cdot I_{stack} \tag{2}$$

$$U_{stack} = n_{cell} \cdot U_{cell} \tag{3}$$

$$I_{stack} = j_{cell} \cdot A_{cell} \tag{4}$$

Instantaneous changes of the process variables can be quantified in terms of absolute change and rate of change. The absolute change $\Delta\Psi$ of an arbitrary process variable Ψ between the time step t_i and the previous time step t_{i-1} can be calculated according to (**5**). From that, the rate of change can be determined by dividing the absolute change by the time resolution following (**6**). For the experiments presented in this article, data logging was limited to a time resolution of 2 s.

$$\Delta\Psi = \Psi(t_i) - \Psi(t_{i-1}) \tag{5}$$

$$\frac{d\Psi}{dt} \approx \frac{\Delta\Psi}{\Delta t} \tag{6}$$

Among all process variables measured during the experiments, current density, cell voltage, electrical stack power, the average temperatures at the stack in and outlets, gas pressures, and separator levels are evaluated using (**5**) and (**6**).

4. Results and discussion

Dynamic operation induces non-stationary operating conditions in water electrolyzers that mainly stem from system inherent inertia and non-ideal process control. These effects of dynamic operation on cell efficiency are not considered whenever steady-state operation is assumed. Deviations from steady-state become much more apparent if the load profile of the electrolyzers contains frequent and pronounced load changes.

4.1. System response to load steps

Artificial rectangular load steps permit an analysis of the system response to well-defined load changes. The temperature profile during the experiment is illustrated in Fig. 3 a). Within the examined current density range, each succession of upward and downward steps causes a characteristic qualitative temperature pattern that reveals the operating point dependent adaption of temperature control. After upward current density steps, the water temperature at the stack exist increases almost instantaneously beyond the set temperature – in this case 75 °C – because of increased heat input by the electrochemical reactions. Due to this temperature deviation, cooling via the heat exchangers is initiated and the temperature decreases following a negative exponential decay. The implemented temperature control of the test-station leads to temperature undershooting due to cooling which is the result of a compromise between fast reaction times and aperiodic control. Overall, the temperature is controlled within −6.7 K and 2.4 K of the nominal temperature. In this experiment, the time interval of 10 min is not sufficient to fully restore the system to set temperature. This leads to a general trend of decreasing temperatures at the end of the cooling step with increasing step height (starting from 4 h). Parallel to the temperature response to upward load changes, a sudden reduction of the current density leads to almost immediately decreasing temperatures at the stack outlet. While the uptake of electrical power by the stacks can be altered very fast, the supplied water is still conditioned according to the heat input at the higher current density, causing decreasing temperatures after downward current density steps.

Fig. 3 b) shows the gas pressure profiles in the anode and cathode compartments during the step experiment. It becomes apparent that the gas pressures are not constant and change immediately after current density steps. Pressure control contains these deviations successfully, but under and overshooting occurs during the settling phase. Interestingly, the absolute deviations from the nominal pressures appear to be independent of the current density step height, indicating the effectiveness of the implemented control scheme. In comparison, pressure control at the anode is more successful, containing the momentary pressure peaks within −0.21 bar and 0.33 bar as opposed −0.50 bar and 0.54 bar at the cathode. This is primarily due to the higher gas flow rates at the cathode, which necessitate faster actuation times of the pressure control valve. Furthermore, the gas pressure stability is affected by the water level control within the gas-water separators.

Under perfectly steady operating conditions, the cell voltage should directly follow the current density profile in galvanostatic mode. Under real experimental conditions however, the cell voltage response becomes progressively unsteady with current density step height and deviates from the ideal rectangular shape of the load profile, as depicted in Fig. 3 c). The cell voltage response exhibits gradually more significant voltage peaks immediately after upward current density steps, reaching a maximum 29 mV as compared to the next operating point. Following these peaks, the cell voltage rapidly decreases although the current density remains constant, before increasing during the 10 min hold time after each step. As these trends are exacerbated by the step height, they arise from transient process values and process control. Downward current density steps exhibit less severe cell voltage peaks and faster settling within the hold time.

Fig. 3 d) illustrates the momentary volume changes within the separators. After upward current density steps, the volume change reaches up to 500 ml, which equals approximately 9.5 % of the nominal separator water volume, due to water surges from the stack to the separator, as discussed in Fig. 2. Downward steps cause less pronounced volume changes of less than 300 ml, which equals 4.9 % of the water volume in the separators. In case of upward current steps, the rapid increase in gas production amplifies the water surge towards the separator. Inversely, water replaces gas volume after downward current density steps, thus not adding additional volume to the two-phase flow. Changes in the separator volume and gas production synchronously add stresses on

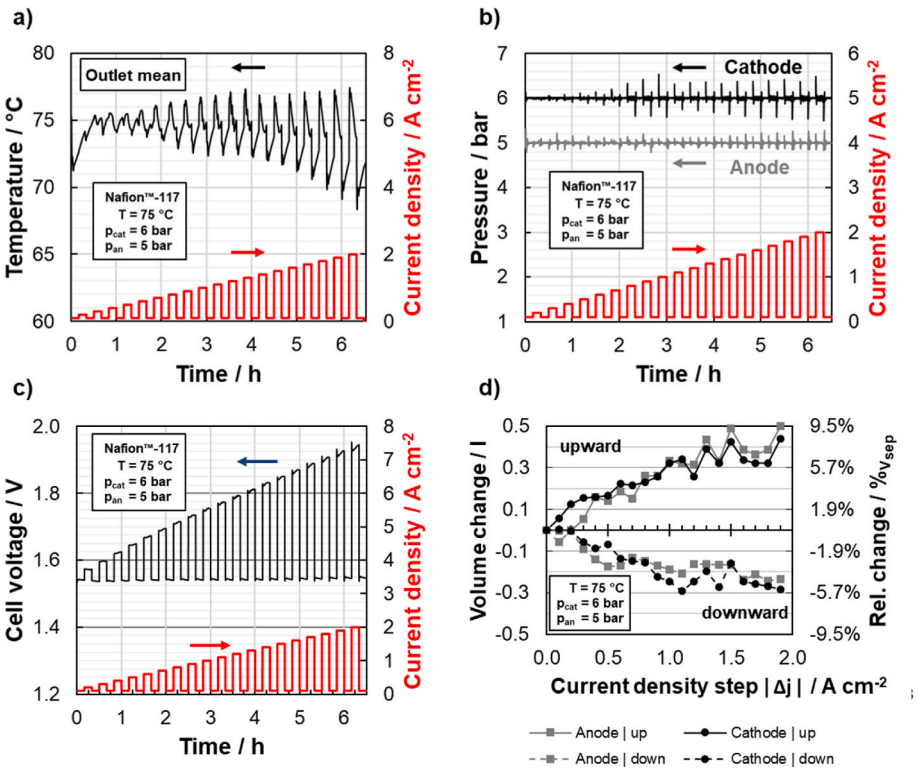

Fig. 3. Step response experiment on the 100 kW_{el} test station: a) mean temperature profile at the stack outlets; b) gas pressure profiles on the cathode (black) and anode (grey) sides; c) mean cell voltage response d) instantaneous volume changes within the cathode (black) and anode (grey) gas-water separators immediately after current density steps from and to 0.10 A cm-2. The separator volume is 9000 cm^3 in both gas cycles and the set filling level is 66 %.

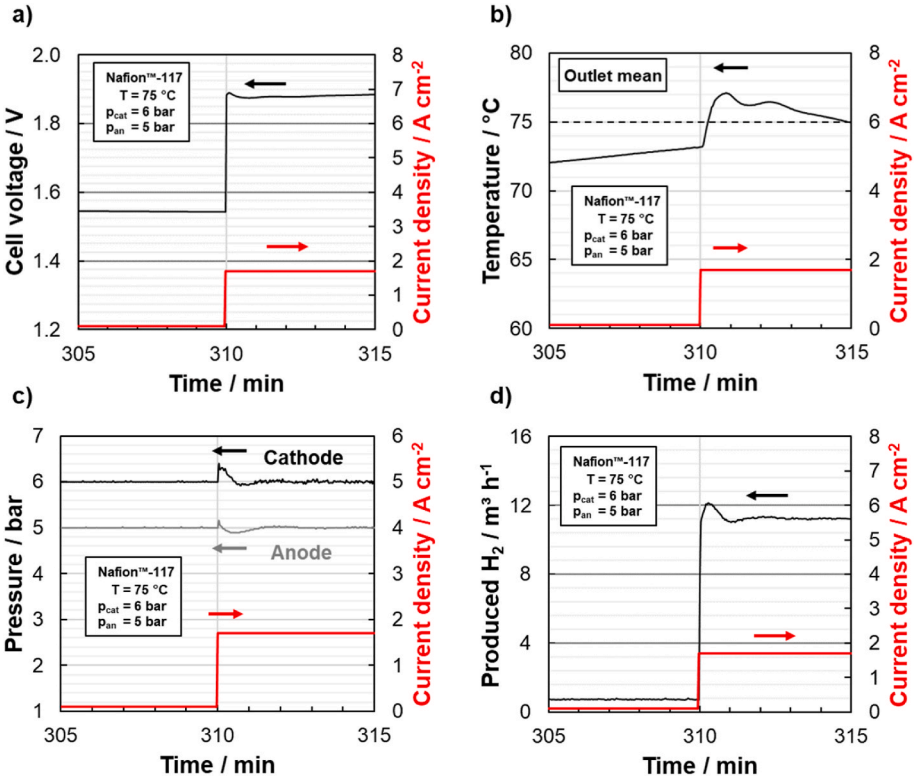

Fig. 4. Exemplary responses of operating parameters during the step response experiment on the 100 kW_{el} test station, for the current density step from 0.10 A cm^{-2} to 1.70 A cm^{-2}: a) mean cell voltage; b) mean temperature at the stack outlets; c) gas pressure profiles on the cathode (black) and anode (grey) sides; d) produced H_2 gas flow, converted to standard conditions at 25 °C and 1.01325 bar.

pressure control that must be considered during pressure control design.

Fig. 4 allows a comparison of the time constants various system postulated in Table 1. As shown in Fig. 4 a), the cell voltage changes instantaneously and reacts within seconds to the change in the current density. However, it takes approximately 4 min for the cell voltage to stabilize. This is mainly due to the temperature control, which becomes apparent in Fig. 4 b), that takes more than 5 min to bring the temperature back to its nominal value. In addition to the fast upward change of temperature, the gas pressures show peaks immediately after the current density steps, as shown in Fig. 4 c). The pressure control is able to stabilize the pressures within seconds, but it takes approximately 1.5 min until the pressures return to their nominal operating points. These pressure peaks contribute to the voltage peaks observed in Fig. 4 a) and may pose further challenges for potential downstream equipment such as compressors and gas dryers. Fig. 4 d) shows the resulting changes in the hydrogen flow at the pressure control valves, which a compressor would have to compensate either by a buffer storage tank or its control scheme. Overall, the time constants agree well with the values stated in Table 1.

4.2. Coupling to renewables

The caracteristics of renewable power genereation are more dynamic and less symetric than the previously discussed synthetic load steps. In the following section direct coupling scenarios to wind power and PV installions are analyzed.

4.2.1. Coupling to wind power

When directly coupled to small-scale wind power installations, the electrolyzers experiences all high-frequency windspeed fluctuations at its electrical power input. Fig. 5 a) depicts the thermal response of the electrolyzer. The mean temperature at the stack exhibits deviations between −3.7 K and 3.2 K from its setpoints. This behaviour is especially apparent during the first 2 h of the experiment, where the current density shifts through the entire part-load range.

Fig. 5 b) depicts the gas pressures in the anode and cathode compartments during the experiment with the wind power profile. The total deviations from the respective pressure setpoints depend on the severity of the power ramps of the load profile. In comparison, the pressure control is shown to be more challenging on the cathode side, where the gas flows are approximately twice as high as on the anode side. On the anode side, pressure deviations range from 0.33 bar to 0.39 bar, while they reach −0.48 bar–0.51 bar on the cathode side. Temperature and pressure control can be improved by control methods such as forward control, which help to reduce instantaneous deviations from the setpoints, as shown by Keller et al. on the same test station [39].

The voltage response of the electrolyzers to the wind power profile is shown in Fig. 5 c). It becomes apparent, that the electrolyzer is able to follow the load pattern, which is especially severe within the first 2 h of the experiment. The electrical power fluctuates between 1.25 kW and 62.23 kW in the current density range from 0.04 A cm^{-2} to 2.00 A cm^{-2}. This causes power ramps between −2.57 kW_{el} s^{-1} and 7.02 kW_{el} s^{-1} between operating points. In terms of power density changes this equals ramps from 1.59 kW_{el} m^{-2} s^{-1} to 4.33 kW_{el} m^{-2} s^{-1}. Fig. 5 d) shows the instantaneous load changes within the separator vessels. Most changes lie in the range of ±100 ml and the linear correlation to the current density step height from Fig. 3 d) is not observed. On the one hand this is due to the significantly smaller step heights in the wind power experiments and on the other hand it is due to the faster operating point changes of the wind power profile, which does not allow the system to settle in its equilibrium.

4.2.2. Coupling to photovoltaics

Photovoltaic electricity production may lead to significant power fluctuations at the electrolysis stack input when direct coupling without buffering components is pursued. Fig. 6 a) shows the mean temperature profiles at the stack in- and outlets in response to the PV current density profile. To maintain the temperature at the outlet within an acceptable range, the water temperature at the stack inlet is adjusted significantly, especially at high current densities between 4 and 10 h of the

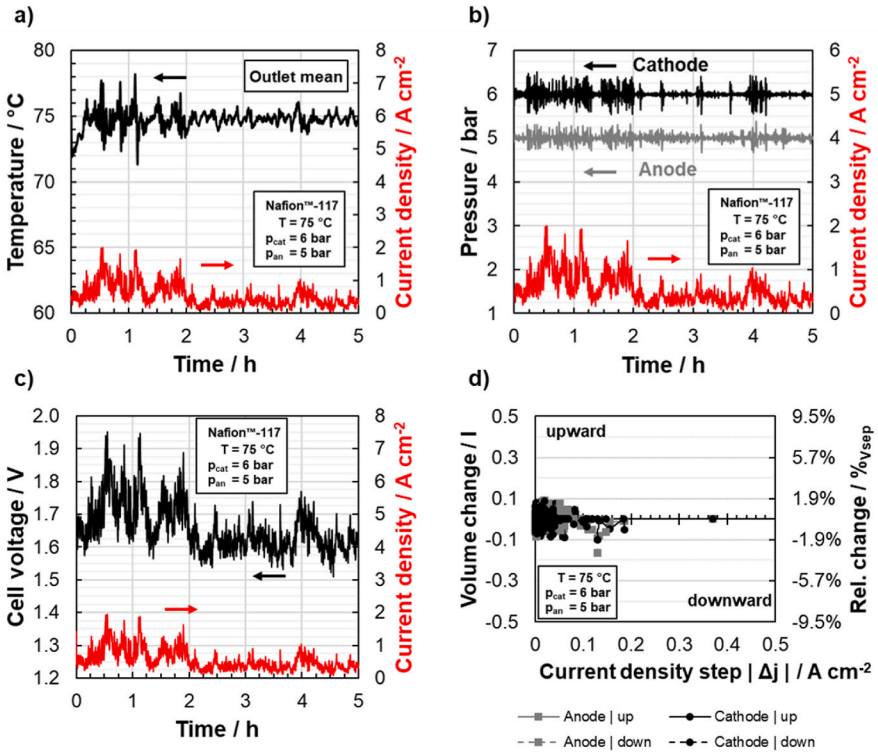

Fig. 5. Coupling to wind power experiment on the 100 kW_{el} test station: a) mean temperature profile at the stack outlets; b) gas pressure profiles on the cathode (black) and anode (grey) sides; c) mean cell voltage response d) instantaneous volume changes within the cathode (black) and anode (grey) gas-water separators.

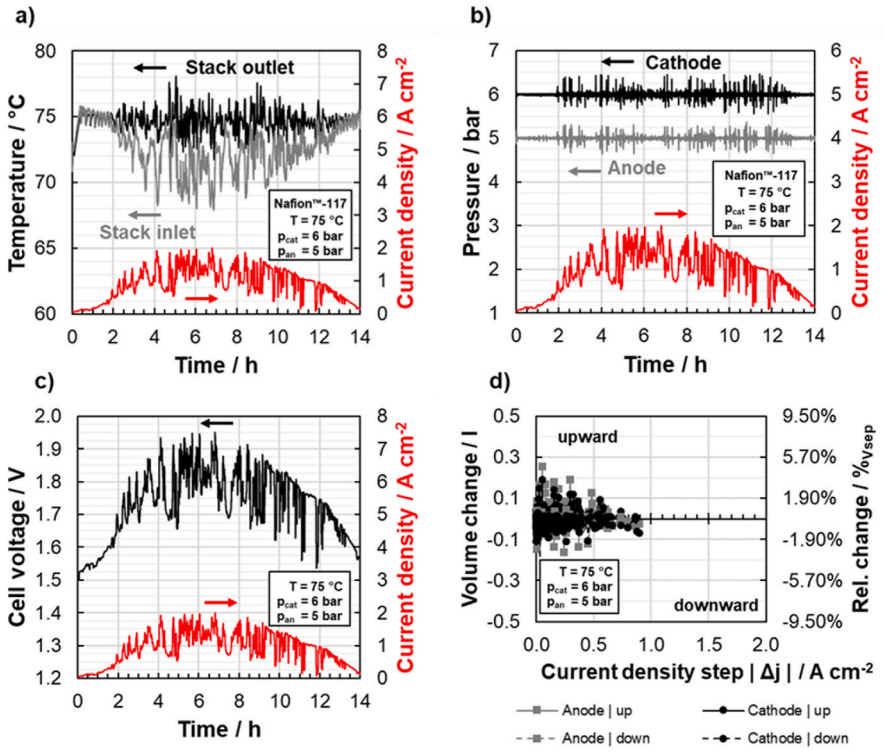

Fig. 6. Coupling to PV experiment on the 100 kW_{el} test station: a) mean temperature profile at the stack outlets; b) gas pressure profiles on the cathode (black) and anode (grey) sides; c) mean cell voltage response d) instantaneous volume changes within the cathode (black) and anode (grey) gas-water separators.

experiment. Maximum deviations of −3.6 K and 3.1 K from the nominal temperature of 75 °C are achieved by reducing the inlet temperature down to 67.9 °C at the highest power density observed during this experiment. Thermal inertia of the cell stacks, the time it takes cool water to flow from the heat exchangers to the stack inlet and mechanical inertia of the cooling water control valve make it difficult to completely prevent instantaneous temperature changes at the stack outlet in dynamic operation. Accordingly, upward power steps are always followed by an increase in cell temperature. Inversely, downward steps are followed by decreasing temperatures. Although these momentary changes are inevitable, the quality of the implemented temperature control scheme determines the time it takes to return the temperature to its setpoint as well as maintaining control stability. Similar reasons lead to the deviations from the gas pressure setpoint, as shown in Fig. 6 b). The gas pressures deviated between 0.35 bar and 0.37 bar on the anode side and between 0.44 bar and 0.48 bar at the cathode side.

Instantaneous mean cell voltage changes range from 198 mV to 180 mV for the highly fluctuating cell voltage profile shown Fig. 6 c). These conditions point to significant electrical stresses of the electrolysis cells during direct coupling with PV installations. Inherently, the entire system must react to the dynamic operation scheme to control process parameters such as stack temperature and gas pressures by adjusting control values. Therefore, non-ideal process control inevitably leads to non-isothermal and non-isobaric operation during dynamic operations. Similar to the observations made on the separator level changes in the wind power experiment, Fig. 6 d) shows that most momentary changes range from ±100 ml.

4.3. Comparison of coupling scenarios

After evaluating all three coupling scenarios separately, a general comparison regarding the observed system dynamics and their consequences on the overall electrolyzer performance can be made. Hereby, intrinsic properties of the characteristic load profiles must be considered. The first basic evaluation criterion is the process efficiency as defined by (1). For the coupling to the renewable energy sources, Fig. 7 gives an overview of the power uptake and efficiency for all load profiles. As the experimentally determined cell efficiency is based on the gas flow measurement after the pressure control valve, momentary values may be exceeding actual values and the efficiency profile temporarily does not match the current density profile. This is mainly due to the dead time behavior of the gas compartment within the electrolyzer and the influence of process control. Nonetheless, Fig. 7 c), d) reveals that the cell efficiency is lower in the volatile, high current density part of the profile within the first 2 h of the experiment, reaching a mean efficiency of 70.64 $\%_{LHV}$ as compared to 75.75 $\%_{LHV}$ for the remaining lower current density part. The mean efficiency is calculated as the average of all measured efficiencies. In total, a mean cell efficiency of 73.70 $\%_{LHV}$ is achieved over the entirety of the wind power experiment. The influence of the system dynamics cannot be easily derived from the efficiency plot, as the gas flow measurement introduces inaccuracy regarding the temporal resolutions. Similar conclusions can be drawn from the efficiency profile for the coupling to PV in Fig. 7 e), f). In the beginning and at the end of the day, the low current densities lead to higher mean efficiencies than in the middle of the day exceeding 75 $\%_{LHV}$. Overall, the mean efficiency of hydrogen production is 71.90 $\%_{LHV}$ for the coupling to PV. Although this value is lower than the mean efficiency for the wind power case, it must be considered that the PV profile relatively contained longer phases at high current densities than the wind power profile. General conclusions about the coupling to wind power and PV cannot be made based on the experimental data presented here. While the wind power profile induces more frequent load changes – due to the higher time resolution of the profile – the PV profile contains more severe instantaneous load changes.

When comparing the coupling scenarios, the observed changes in the process variables and the resulting electrical properties can be differentiated. Table 3 gives an overview of the absolute changes in the process variables and the frequency distribution of the observed changes. The absolute changes in mean temperature and gas pressures have been discussed under the respective experiments in Section 4.1 and Section

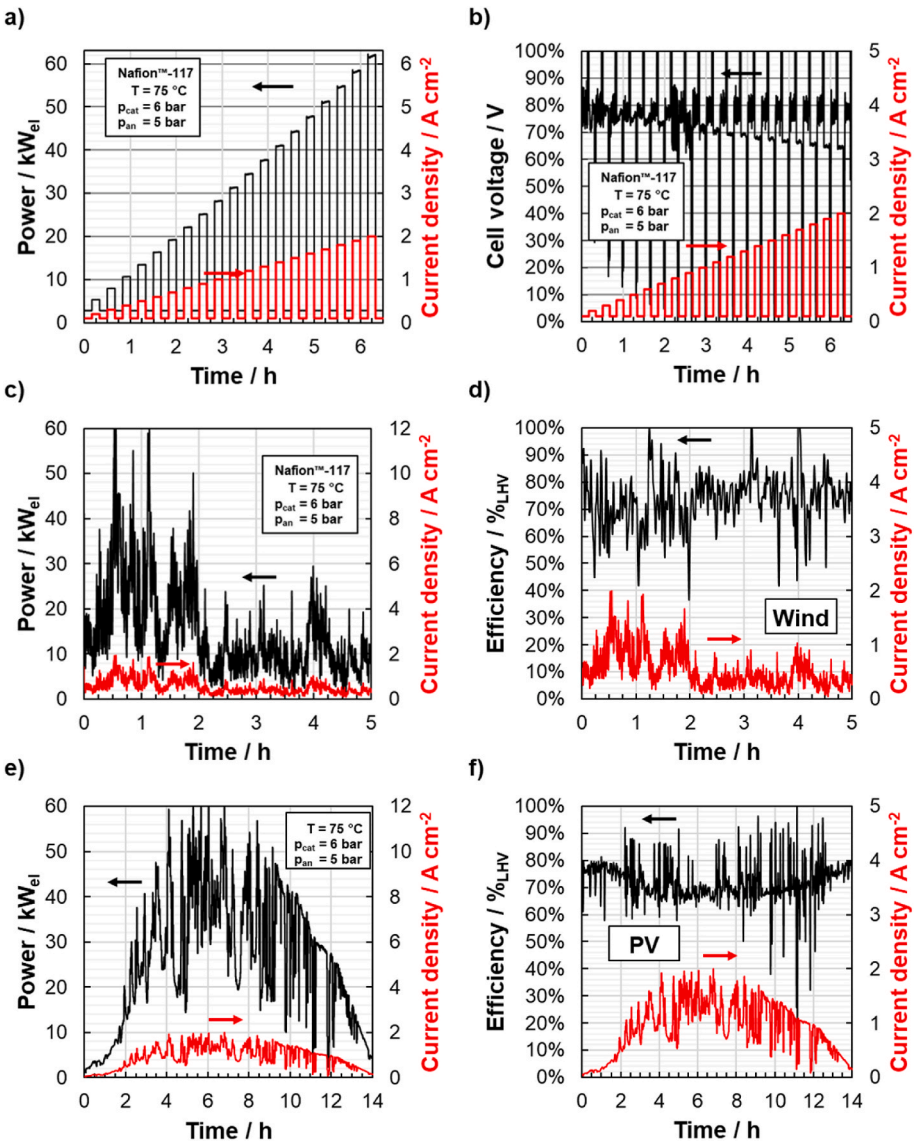

Fig. 7. Comparison of the power uptake and hydrogen production efficiencies at the 100 kW_{el} test station: a),b) for the synthetic step profile; c),d) for the wind power profile and e),f) for the PV profile.

Table 3
Process variable deviations from their nominal setpoints during the experiments. For the calculation of the deviations, the data logging time resolution of 2 s was utilized.

		Step profile	Wind power	Photovoltaics
Mean temperature	ΔT (min./max.)	−6.66/2.44 K	−3.68/3.19 K	−3.63/3.10 K
	±1 K	61.0%	93.2%	89.2%
	±2 K	82.1%	97.8%	98.0%
Pressure -Anode	Δp (min./max.)	−0.21/0.33 bar	−0.33/0.39 bar	−0.35/0.37 bar
	±0.1 bar	97.0%	83.5%	92.0%
	±0.2 bar	99.3%	96.3%	97.4%
Pressure -Cathode	Δp (min./max.)	−0.50/0.54 bar	−0.48/0.51 bar	−0.44/0.48 bar
	±0.1 bar	95.9%	82.3%	94.9%
	±0.2 bar	98.1%	91.8%	98.1%

4.2. In addition to that, the frequency distribution of discrete changes has been evaluated, giving an impression of the probability of encountering such changes in similar scenarios. In comparison, the instantaneous temperature changes are highest in the artificial step profile, which is due to the significantly higher current density step heights in this experiment. In contrast, the wind power and PV profile lead to similar maximum temperature changes within ±4 K. While only 82.1% of the instantaneous changes in mean cell temperature lie in the ±2 K range during the step experiment, 97.8% and 98.0% do so for the experiments with the RE profiles. The pressure data in Table 3 supports the overall observation, that pressure control at the cathode side is more challenging, because on the one hand the momentary absolute pressure deviations are always higher and more frequently exceed the ±0.2 bar range. Nonetheless, except for the pressure deviations at the cathode during the wind power experiment, more than 96% of all pressure changes lie within the ±0.2 bar range. Therefore, only exceptionally severe operating point changes lead to peaks in the process values and process control can stabilize them appropriately for most of the experiments.

Changes in the process values directly influence the electrical process properties of the electrolyzer such as the cell voltage and the resulting power ramps. In galvanostatic operation, the absolute changes in cell voltage mainly depend on the underlying current density profile and the absolute changes thereof. Dynamic operation however exacerbates the

cell voltage shifts compared to the expected response during steady-state operation as Fig. 3 illustrates. Interestingly, based on the cell voltage changes in Table 4, there appears to be a correlation between absolute current density changes and the momentary voltage shifts. During the step profile experiments, the voltage changes are roughly twice as high as the changes during the PV profile, which translates to the current density profile. In contrast to that, the wind power profile has even lower current density step heights and induces much lower changes in cell voltage still.

Regardless of the analyzed scenario, voltage peaks are experienced seldomly and more than 99 % of the voltage changes lie within ±20 mV. However, this frequency distribution is affected by the time resolution of the load profile, which explains the lower share of small voltage shifts in the wind power experiment, where the settling time was shortest with 1 s, this settling time is in accordance with the observations from Immerz et al. [27]. As the power uptake of the cell stacks is directly connected to current density and cell voltage, the power ramps in Table 4 follow the qualitative observations discussed for the cell voltage. Because of the synthetic nature of the step profile and the settling time of 10 min during the experiments, the frequency distributions of cell voltage and power ramps are identical with 99.7% of all momentary changes lying within ±20 mV and ±1.0 kW s^{-1}.

Hydrogen production is influenced by all changes in the operating parameters and dynamic operation affects the efficiency depending on the individual operating point positively or negatively. Although a general judgment in terms in efficiency is therefore not possible, the efficiency more likely decreases in dynamic operation compared to steady-state operation. This conclusion is based on Table 3, where the instantaneous changes in cell temperature below the setpoint are more pronounced than those above the setpoint for all coupling scenarios. If near isobaric conditions are assumed, lower temperatures lead to lower cell efficiencies.

4.4. Strategies to mitigate limitations due to system dynamics

Although system dynamics due to transient operating states inevitably in water electrolyzers during coupling to volatile electricity sources, several strategies can help to mitigate limitations on efficiency and operability. Either the design of the electrolyzer and its components or the operation strategy can be adapted.

4.4.1. Adaption of the electrolyzer design

As discussed above, each component of the water electrolyzer provides specific inertia to the entire system. Accordingly, increasing the volume of peripherals such as water separators or pipes increases the thermal inertia of the system while simultaneously increasing transit times between components, which makes process control more difficult.

Table 4
Electrical responses of the cell stacks to operating point changes during the experiments. For the calculation of the deviations, the data logging time resolution of 2 s was utilized.

		Step profile	Wind power	Photovoltaics
Cell voltage	ΔU (min./max.)	−407/395 mV	−30/99 mV	−198/180 mV
	±10 mV	99.7%	94.3%	98.7%
	±20 mV	99.7%	99.2%	99.0%
Power ramp	dP/dt (min./max.)	−29.58/29.51 kW s^{-1}	−2.57/7.02 kW s^{-1}	−15.22/13.54 kW s^{-1}
	dP'/dt (min./max.)	−18.3/18.2 kW m^{-2} s^{-1}	−1.6/4.3 kW m^{-2} s^{-1}	9.4/8.4 kW m^{-2} s^{-1}
	±0.5 kW s^{-1}	99.7%	90.4%	98.4%
	±1.0 kW s^{-1}	99.7%	97.6%	98.8%

Ensuring an appropriate size of the separators must consider the water surges during dynamic operation to prevent critical operating states caused by vessel overflow or emptying. For example, during the synthetic step profile experiment, an empty head-space in the water separators of at least17 ml s kW_{el}^{-1} – or 142 ml cm^2 W_{el}^{-1} in terms of power density ramps – was required to buffer the occurring water surges. Larger separators also buffer thermal transients because of their higher heat capacity and stabilize the pressure control. A compromise between investment costs, footprint and functionality must be found for each use-case. On the one hand, the piping within the water cycles should be kept as short as possible to reduce transit times of fluids between components. On the other hand, increasing the pipe length in the gas cycle or including gas buffer tanks, which could act as condensate trap, can smoothen the gas pressure dynamics because of the larger gas volume. Furthermore, placing the heat exchangers and a potential heating close to the stack inlet is favorable, as it makes temperature control faster and more effective.

On the stack side, it could be beneficial to integrate more functions of the peripheral components within the stack. Adding cooling plates to the stack or realizing gas-water separation directly at the stack would move the thermal inertia of peripherals closer to the sites of heat production or demand. This would reduce transit times and dampen thermal spikes that are inevitable in dynamic operation. These benefits would however lead to more complex stack designs and make stack servicing, ensuring gas tightness and process safety more challenging.

4.4.2. Adaption of the operation strategy

The experimental results in this study suggest that isothermal, isobaric conditions are unachievable in dynamic operation. Nonetheless, developing improved process control schemes can increase stability during operation and reduce stress on adjoining systems. Controlling the maximum temperature is mandatory to prevent thermal degradation of the electrolytic membrane and should always be considered during the control design process. In terms of process efficiency, it might even be favorable to allow temperature decreases due to load point changes, as the highest operating temperature not necessarily maximizes efficiency [46]. Other adaptions of the operating strategy aim at reducing the dynamics of the electrical power input. This could be achieved by smart interaction with the electricity grid – if possible – or utilization of electrical buffer storages such as batteries or supercapacitors. Additionally, in case of larger electrolysis installations with several stacks, smart on and off switching of electrolysis stacks can optimize the part-load operation.

5. Conclusions

Regarding the consequences of dynamic operation on water electrolyzers, several conclusions can be drawn based on this study. Overall, the deciding factors on system dynamics are the severity of load point changes, as well as the ability of the system to follow these changes. Accordingly, the synthetic rectangular step profile was the most challenging, followed by the PV profile. Drastic load changes due to cloud movement cause harsher system dynamics than fast load point shifts due to wind speed changes. Due to their dependence on varying system inertias and underlying mechanisms, process variables react differently to the operating point changes. Although isothermal and isobaric operation is impossible, adequate design of process control enhances process stability and safety. Temperature control appears most challenging, based on the relative deviations between −6.7 K and 3.2 K from their setpoint during experiments on the 100 kW_{el} system. Pressure control at the cathode side is more demanding compared to the anode side, reaching deviations of −0.50 bar–0.54 bar, as compared to between −0.33 bar and 0.39 bar at the anode. The electrical performance of the electrolyzer is mostly influenced by the operating profile and its absolute changes as well as settling times. Water electrolyzers offer a high degree of flexibility for grid stability tasks and power ramps of ±30 kW_{el} s^{-1}

were observed experimentally. Based on the experimental data from the test station, under the given operating parameters and process control, it is concluded that temperature dips during dynamic operation lower the mean hydrogen production efficiency as compared to steady state. Coupling to wind power was observed to be more efficient, reaching a mean efficiency of 73.70 $\%_{LHV}$, than coupling to PV installations which yielded 71.90 $\%_{LHV}$. Potential adaptions of electrolyzer designs and operation strategies were discussed, which can benefit system designers and operators in practical applications.

Credit authorship contribution statement

Conceptualization: E.R. and M.M.; methodology: E.R., M.H.; resources: M.H.; writing—original draft preparation: E.R.; writing—review and editing: F·S., M.H., and M.M.; visualization: E.R.; supervision: M.M., R.P., and D.S. All authors have read and agreed to the published version of the manuscript.

Declaration of competing interest

The authors declare the following financial interests/personal relationships which may be considered as potential competing interests:

Edward Rauls reports financial support was provided by European Regional Development Fund (ERDF).

Acknowledgements

This work was supported by the state of North Rhine–Westphalia with funds from the European Regional Development Fund (ERDF) as part of the project, “Kompetenz-Zentrum Virtuelles Institut Strom zu Gas und Waerme” (Grant No. EFRE-0400151) and by the Deutsche Forschungsgemeinschaft (DFG, German Research Foundation) - 491111487. The authors would also like to thank Roger Keller, Walter Zwaygardt and Richard Wegner for their support during the experiments.

Appendix A. Supplementary data

Supplementary data to this article can be found online at https://doi.org/10.1016/j.ijhydene.2024.03.302.

Nomenclature

Latin symbols	*Meaning*	*Unit*
A	cell area	cm^2
I	current	A
j	current density	$A\ cm^{-2}$
LHV	lower heating value	$kJ\ kg^{-1}$
n	number of cells	-
P	power	kW
T	temperature	K
t	time	s
U	voltage	V
V	volume	m^3

Greek symbols	*Meaning*
Δ	absolute difference
η	efficiency %
Ψ	arbitrary variable

Subscripts	*Meaning*
an	anode
cat	cathode
el	electric
H_2	hydrogen

References

[1] Diesendorf M, Elliston B. Renew Sustain Energy Rev 2018;93:318–30. https://doi.org/10.1016/j.rser.2018.05.042.
[2] Mlilo N, Brown J, Ahfock T. Technol econ smart grids. Sustain Energy 2021;6. https://doi.org/10.1007/s40866-021-00123-w.
[3] Blanco H, Faaij A. Renew Sustain Energy Rev 2018;81:1049–86. https://doi.org/10.1016/j.rser.2017.07.062.
[4] Ruhnau O, Qvist S. Environ Res Lett 2022;17:44018. https://doi.org/10.1088/1748-9326/ac4dc8.
[5] Engeland K, Borga M, Creutin J-D, François B, Ramos M-H, Vidal J-P. Renew Sustain Energy Rev 2017;79:600–17. https://doi.org/10.1016/j.rser.2017.05.046.
[6] Anvari M, Lohmann G, Wächter M, Milan P, Lorenz E, Heinemann D, Tabar MRR, Peinke J. New J Phys 2016;18:63027. https://doi.org/10.1088/1367-2630/18/6/063027.
[7] Mladenov V, Chobanov V, Georgiev A. Energies 2021;14:2813. https://doi.org/10.3390/en14102813.
[8] Luderer G, Madeddu S, Merfort L, Ueckerdt F, Pehl M, Pietzcker R, Rottoli M, Schreyer F, Bauer N, Baumstark L, Bertram C, Dirnaichner A, Humpenöder F, Levesque A, Popp A, Rodrigues R, Strefler J, Kriegler E. Nat Energy 2022;7:32–42. https://doi.org/10.1038/s41560-021-00937-z.
[9] Petinrin JO, Shaabanb M. Renew Sustain Energy Rev 2016;65:770–83. https://doi.org/10.1016/j.rser.2016.06.073.
[10] Milligan M. Electr J 2018;31:1–7. https://doi.org/10.1016/j.tej.2018.10.002.
[11] Allidières L, Brisse A, Millet P, Valentin S, Zeller M. Int J Hydrogen Energy 2019;44:9690–700. https://doi.org/10.1016/j.ijhydene.2018.11.186.
[12] Bergen A, Pitt L, Rowe A, Wild P, Djilali N. Int J Hydrogen Energy 2009;34:64–70. https://doi.org/10.1016/j.ijhydene.2008.10.007.
[13] Sartory M, Wallnöfer-Ogris E, Salman P, Fellinger T, Justl M, Trattner A, Klell M. Int J Hydrogen Energy 2017;42:30493–508. https://doi.org/10.1016/j.ijhydene.2017.10.112.
[14] Calnan S, Bagacki R, Bao F, Dorbandt I, Kemppainen E, Schary C, Schlatmann R, Leonardi M, Lombardo SA, Milazzo RG, Privitera SMS, Bizzarri F, Connelli C, Consoli D, Gerardi C, Zani P, Carmo M, Haas S, Lee M, Mueller M, Zwaygardt W, Oscarsson J, Stolt L, Edoff M, Edvinsson T, Pehlivan IB. Sol RRL 2022;6:2100479.
[15] Ghosh PC, Emonts B, Janßen H, Mergel J, Stolten D. Sol Energy 2003;75:469–78. https://doi.org/10.1016/j.solener.2003.09.006.
[16] Gazey R, Salman SK, Aklil-D'Halluin DD. J Power Sources 2006;157:841–7. https://doi.org/10.1016/j.jpowsour.2005.11.084.

[17] Ulleberg Ø, Nakken T, Eté A. Int J Hydrogen Energy 2010;35:1841–52. https://doi.org/10.1016/j.ijhydene.2009.10.077.
[18] Stansberry JM, Brouwer J. Int J Hydrogen Energy 2020;45:9305–16. https://doi.org/10.1016/j.ijhydene.2020.01.228.
[19] Clarke RE, Giddey S, Ciacchi FT, Badwal S, Paul B, Andrews J. Int J Hydrogen Energy 2009;34:2531–42. https://doi.org/10.1016/j.ijhydene.2009.01.053.
[20] Clarke DP, Al-Abdeli YM, Kothapalli G. Int J Hydrogen Energy 2013;38:12253–65. https://doi.org/10.1016/j.ijhydene.2013.07.031.
[21] Kopp M, Coleman D, Stiller C, Scheffer K, Aichinger J, Scheppat B. Int J Hydrogen Energy 2017;42:13311–20. https://doi.org/10.1016/j.ijhydene.2016.12.145.
[22] Chen M, Chou S-F, Blaabjerg F, Davari P. Appl Sci 2022;12:1906. https://doi.org/10.3390/app12041906.
[23] Weng D, Wainright JS, Landau U, Savinell RF. J Electrochem Soc 1996;143:1260–3. https://doi.org/10.1149/1.1836626.
[24] Stiber S, Sata N, Morawietz T, Ansar SA, Jahnke T, Lee JK, Bazylak A, Fallisch A, Gago AS, Friedrich KA. Energy Environ Sci 2022;15:109–22. https://doi.org/10.1039/D1EE02112E.
[25] Maier M, Smith K, Dodwell J, Hinds G, Shearing PR, Brett D. Int J Hydrogen Energy 2022;47:30–56. https://doi.org/10.1016/j.ijhydene.2021.10.013.
[26] Müller M, Carmo M, Glüsen A, Hehemann M, Saba S, Zwaygardt W, Stolten D. Int J Hydrogen Energy 2019;44:10147–55. https://doi.org/10.1016/j.ijhydene.2019.02.139.
[27] Immerz C, Bensmann B, Trinke P, Suermann M, Hanke-Rauschenbach R. J Electrochem Soc 2019;166:F1200–8. https://doi.org/10.1149/2.0881914jes.
[28] Mohanpurkar M, Luo Y, Terlip D, Dias F, Harrison K, Eichman J, Hovsapian R, Kurtz J. Energies 2017;10. https://doi.org/10.3390/en10111836.
[29] Teuku H, Alshami I, Goh J, Masdar MS, Loh KS. Int J Energy Res 2021;45:20583–600. https://doi.org/10.1002/er.7182.
[30] Panchenko O, Borgardt E, Zwaygardt W, Hackemüller FJ, Bram M, Kardjilov N, Arlt T, Manke I, Müller M, Stolten D, Lehnert W. J Power Sources 2018;390:108–15. https://doi.org/10.1016/j.jpowsour.2018.04.044.
[31] Minnaar C, de Beer F, Bessarabov D. Energy Fuels 2020;34:1014–23. https://doi.org/10.1021/acs.energyfuels.9b03814.
[32] Rakousky C, Reimer U, Wippermann K, Kuhri S, Carmo M, Lueke W, Stolten D. J Power Sources 2017;342:38–47. https://doi.org/10.1016/j.jpowsour.2016.11.118.
[33] Weiß A, Siebel A, Bernt M, Shen TH, Tileli V, Gasteiger HA. J Electrochem Soc 2019;166:F487–97. https://doi.org/10.1149/2.0421908jes.
[34] Alia SM, Stariha S, Borup RL. J Electrochem Soc 2019;166:F1164–72. https://doi.org/10.1149/2.0231915jes.
[35] Frensch SH, Fouda-Onana F, Serre G, Thoby D, Araya SS, Kær SK. Int J Hydrogen Energy 2019;44:29889–98. https://doi.org/10.1016/j.ijhydene.2019.09.169.
[36] Speckmann F-W, Bintz S, Birke KP. Appl Energy 2019;250:855–63. https://doi.org/10.1016/j.apenergy.2019.05.014.
[37] Yodwong B, Guilbert D, Phattanasak M, Kaewmanee W, Hinaje M, Vitale G. Electronics 2020;9. https://doi.org/10.3390/electronics9060912.
[38] Koponen J, Ruuskanen V, Hehemann M, Rauls E, Kosonen A, Ahola J, Stolten D. Appl Energy 2020;279:115791. https://doi.org/10.1016/j.apenergy.2020.115791.
[39] Keller R, Rauls E, Hehemann M, Müller M, Carmo M. Control Eng Pract 2022;120:104992. https://doi.org/10.1016/j.conengprac.2021.104992.
[40] Rauls E, Hehemann M, Keller R, Scheepers F, Müller M, Stolten D. Appl Energy 2023;330:120350.
[41] Sircar S, Golden TC. Separ Sci Technol 2000;35:667–87. https://doi.org/10.1081/SS-100100183.
[42] Tjarks G, Gibelhaus A, Lanzerath F, Müller M, Bardow A, Stolten D. Appl Energy 2018;218:192–8. https://doi.org/10.1016/j.apenergy.2018.02.155.
[43] Sdanghi G, Maranzana G, Celzard A, Fierro V. Renew Sustain Energy Rev 2019;102:150–70. https://doi.org/10.1016/j.rser.2018.11.028.
[44] Gorre J, Ruoss F, Karjunen H, Schaffert J, Tynjälä T. Appl Energy 2020;257:113967. https://doi.org/10.1016/j.apenergy.2019.113967.
[45] Tang C, Soong WL, Freere P, Pathmanathan M, Ertugrul N. Wind Energ 2013;16:561–73.
[46] Scheepers F, Stähler M, Stähler A, Rauls E, Müller M, Carmo M, Lehnert W. Appl Energy 2021;283:116270. https://doi.org/10.1016/j.apenergy.2020.116270.